Rev. Roum. Sci. Techn.– Électrotechn. et Énerg.
Vol. **62**, *4*, pp. 424–430, Bucarest, 2017

Termotechnique et termoénergétique

NUMERICAL SIMULATION OF HEAT TRANSFER PROCESS IN A NON-CONVENTIONAL CALORIMETER

JORGE M. CRUZ-DUARTE[1], ALEXANDRU M. MOREGA[2], ARTURO GARCIA-PEREZ[1], C. RODRIGO CORREA-CELY[3]

Key words: Calorimetry, Thermal management, Numerical simulation, Power losses estimation, Heat transfer.

This article proposes a non-conventional calorimeter for the power losses quantification of microelectronic devices during their operation. The system is based on the constant-volume calorimetry principle, mainly employed in bio-chemical applications. Additionally, this document presents a primary numerical study for proposed device. Several experiments were conducted to observe the heat transfer performance inside the system. Results were found useful for the eventual practical implementation.

1. INTRODUCTION

Thermal management in microelectronic components is a well-known problem for electronic designers, engineers, or technicians. In most practical cases, this problem remains partially attended by electronic specialists and engineering students due to uncountable reasons. Nonetheless, there exists a colossal number of strategies aimed at besieging this problem, though, heat sinks or heat pipes are recurrent solutions for microelectronic devices [1, 2]. But, those mechanical solutions are effectively implemented on microelectronic devices with known thermal behaviours. In other words, the power losses have been previously studied and quantified.

Measurement of the electronic power losses, say the net heat power generation, is considered into design thermal management solutions for specific cases. Multiple paths to accomplish an accurate model for the thermal behaviour of several engineering systems have been proposed. For the case of electrical/electronic components, these strategies can be categorised in two groups: *the electrical* and *the calorimetric methods* [3, 4]. These methods have a recognised trade-off between results accuracy and implementation difficulty. That is, the former has results with high uncertainty but it is easy to implement, conversely, the latter has high accuracy with an associated high complexity of implementation [5]. The electrical method founds on the estimation of power losses by employing electrical measured variables such as current and voltage. Besides, *the calorimetric method* consists on the directly determination of the power losses from a specific system utilising a characterised substance, by measuring changes in its state variables [6, 7]. Thus, a calorimeter is chiefly composed by the system under test and the characterised substance, both thermally connected and inside an insulation coat. The substance is commonly a fluid flow through the system, or in a heat exchanger inside it [4]. Both setups are grouped employing the thermodynamic sense of a system, *i.e.*, open, and closed systems. Further, *the double-jacketed calorimeters* constitute a special case of the closed type [3]. Those enhance the accuracy and performance of an open type calorimeter by enclosing its surroundings in a closed system.

Multiple implementations of calorimeters can be found in literature. Although, calorimeters with fluid flows, like the double-jacketed one, are widely used. It is mainly due their response time is shorter than closed ones, but consuming an additional pumping power. Most of them have aimed at the power losses estimation of electrical devices. Some examples of those are presented as follows. Blaabjerg *et al.* presented a measuring system for industrial and home components [8]. Malliband *et al.* quantified power generation from an inverter at different switching frequencies [9]. Weier *et al.* implemented a conventional calorimeter for mobile phone chargers and lamp ballasts [10]. Christen et al. studied the energetic measurement in a power converter system [11]. Moreover, some authors have modified the calorimeter schema by integrating alternative components to enhance their performance. Marín *et al.* implemented a system for microelectronic circuits, with the test chamber immersed in a distilled water body, whilst it was mixing by a paddle-wheel [12]. Frost and Howey constructed a high-speed calorimeter for electronic elements. They put Peltier's element at the coolers, and tuned the system with artificial neuronal networks [13].

This work proposes a non-conventional calorimeter for electronic devices, and presents its primary numerical simulations and analyses. The system consists in a vertical cylindrical concentric cavity, based on the constant-volume calorimetry principle widely used in biology and chemical applications [6], and implemented for electronic devices [12]. Moreover, it aims to be a low cost and efficient tool for electronic designers, students, and related people. Several numerical experiments were conducted chiefly to find locations for temperature sensors, and to observe the heat transfer performance inside the system. Results obtained in this study are useful for the eventual implementation and instrumentation of the calorimeter. This document is organised as follows. Section 2 displays foundations about calorimetry. Section 3 describes the mathematical model of the proposed system. Subsequently, methodology and results are discussed. Finally, most important highlights are summarised in Conclusions.

2. FOUNDATIONS

The principle of calorimetry is based on a generalisation of the Joule's experiment, and the specific heat (c [J/kg · K]) value of a system, at a reference temperature (T_0 [K]),

$$c := \left.\frac{\partial h}{\partial T}\right|_{T=T_0}, \tag{1}$$

since h [J/kg] is the enthalpy energy, and T [K] is its

[1] University of Guanajuato, Salamanca, Mexico, E-mail: {jorge.cruz, arturo}@ugto.mx
[2] "Politehnica" University of Bucharest, Bucharest, Romania, E-mail: amm@iem.pub.ro
[3] Industrial University of Santander, Bucaramanga, Colombia, E-mail: crcorrea@uis.edu.co

absolute temperature [14]. It estimates the amount of energy which is generated for process, by measuring changes of temperature in a *storage* system, with known thermophysical properties [6–9]. Temperature variations are assumed as uniformly and isothermally in function of the time [15]. Thus, the calorimeter behaviour can be modelled through the lumped capacitance method [16, 17]. It means the thermal system is modelled utilising the electrical circuits analogy. For this work, a simplest model with an equivalent thermal resistance (R [K/W]) and a thermal capacity (C [J/K]) is analysed. The effective thermal power ($\dot{Q}$ [W]) is represented as the flow source, and the temperature difference ($\theta = T - T_0$ [K]) as the effort. Reference temperature difference equals zero. Hence, an initial value problem can be formulated by analysing the main node θ, such as

$$\frac{\mathrm{d}\theta(t)}{\mathrm{d}t} + \frac{\theta(t)}{\tau} = \frac{\dot{Q}}{C}, \quad \forall t \geq 0, \quad \theta(t=0) = 0, \tag{2}$$

with $\tau = RC$ [s] as the time constant of the system. The solution of this problem is given by,

$$\theta(t) = \theta_\infty \left(1 - \exp\left\{-\frac{t}{\tau}\right\}\right), \tag{3}$$

where $\theta_\infty = \tau\dot{Q}/C$ is the final value of eq. (3) when $t \to \infty$, or the steady state response. Thus, a formula for the equivalent thermal resistance of the system, in stationary state, is found as

$$R = \frac{\theta_\infty}{\dot{Q}}. \tag{4}$$

The value of R can be approached by experimental or numerical data, or by utilising a comprehensive theoretical model based on heat transfer foundations. Many works have demonstrated that R chiefly includes heat transport mechanisms like convection and conduction [15–17]. This model requires a most detailed analysis in transient state.

Other relevant relationship can be extracted from the initial slope of $\theta(t)$, in eq. (3)

$$\left.\frac{\mathrm{d}\theta(t)}{\mathrm{d}t}\right|_{t=0} = \frac{\theta_\infty}{\tau} = \frac{\dot{Q}}{C}. \tag{5}$$

Equation (5) brings to light a hint of what could be the expression for heat power estimation. Using eq. (1) and the first law of thermodynamic for a constant-volume closed quasi-static system [14], it is obtained the thermal capacity as

$$C = \rho c V. \tag{6}$$

C in eq. (6) depends of properties such as, the mass density, ρ [kg/m^3], the specific heat, c [J/kg·K], and the volume, V [m^3], of substance serving as energy storage.

The characterisation of a calorimetric system can be a hard work for practical implementations, mainly in terms of the equivalent thermal resistance model. Nevertheless, it is possible to reduce the complexity of eq. (2), by defining external boundaries of the entire system as adiabatic, *i.e.*, $R \to \infty$. It can be achieved by utilising composites with excellent insulation properties. Thus, eq. (2) yields

$$\dot{Q} \approx \rho c V \frac{\mathrm{d}\theta(t)}{\mathrm{d}t}, \tag{7}$$

where $\dot{Q}$ [W] is the estimated electronic power losses.

3. MATHEMATICAL MODEL

The proposed non-conventional calorimeter device is presented in Fig. 1, which presents its entire domain and its symmetry-based reduced domain. The reduced system is defined as a slice of the entire system, which contains a half fin and channel of the radial fin array at the main chamber.

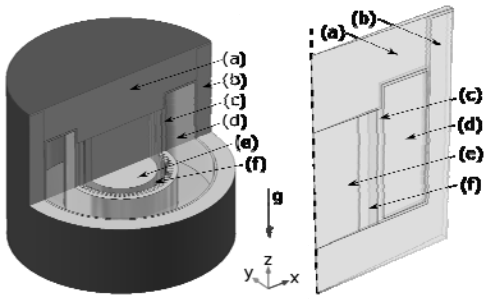

Fig. 1 – Computational domains of the studied system, a non-conventional calorimeter for electronic devices: (left) entire, and (right) symmetry-based reduced domains.

All subdomains (Fig. 1) are described as follows: a) *Insulation cover* allows locate the electronic device to be analysed in the main chamber and, also, serves as an insulation wall; b) *Insulation coat* insulates the process of any external thermal perturbation; c) *Conductive core* is the thermal conductive metallic body which is made by a radial plate-fin heat sink (the main chamber) and a fluid reservoir; d) *Working fluid* exerts as a thermal energy storage body, e) *Heat source* is the unknown electronic device under analysis inside the main chamber; in this work, it is assumed as a cylindrical body for illustrative purposes; f) *Air gap* is the gap between the electronic device and the main chamber. In addition, Table 1 presents thermophysical properties of materials and fluids, linked to the above-mentioned subdomains, considered in this work.

Table 1

Thermophysical properties of materials used in this work

Subdomain	Material	Property	Value
(a)–(b)	Polystyrene (PS)	ρ	28 kg/m^2
		k	0.033 W/m·K
		c	1500 J/kg·K
(c)	Aluminium (Al)	ρ	2700 kg/m^2
		k	238 W/m·K
		c	900 J/kg·K
(d)	Water (H_2O)	ρ	998.2 kg/m^2
		k	0.615 W/m·K
		c	4182.6 J/kg·K
		μ	8.5×10^{-4} Pa·s
		β	2.75×10^{-4} 1/K
		γ (1)	1
(e)	FR4	ρ	1900 kg/m^2
		k	0.3 W/m·K
		c	1369 J/kg·K
(f)	Air	ρ	1.1839 kg/m^2
		k	0.25 W/m·K
		c	1004 J/kg·K
		μ	1.4×10^{-5} Pa·s
		β	3.355×10^{-3} 1/K
		γ	1.4

(1) Ratio of specific heats

To model the stationary and transient behaviour of both models of the calorimetric system presented in Fig. 1, the mathematical problem is described as follows. On practical engineering systems, it is common to start analysing the operating process employing the mass conservation principle, also known as the continuity equation [15, 16]. In this work, the mass density for both fluids in the system (*i.e.*, air and water) is assumed constant, hence

$$\rho(\nabla \cdot \mathbf{u}) = 0, \tag{8}$$

which means that the mass inside the system remains invariant in both stationary and transient states. This expression is associated to the incompressible flow condition either.

Next modelling step deals with the energetic interaction in the operating system, that is through the first law of thermodynamics [14–19]. It is important to remember that heat transfer is the main physical phenomenon of the computational model. Other interactions like changes on the kinetic and potential energy are neglected. Thus, the energy balance per unit volume for all domains of the model (Fig. 1) is presented as

$$\frac{1}{\alpha}\left[\frac{\partial T}{\partial t} + (\mathbf{u}\cdot\nabla)T\right] = \nabla^2 T - \frac{\mathbf{q}_e}{k}, \tag{9}$$

where $\alpha = k/\rho c$ [m^2/s] is the thermal diffusivity, c [J/kg · K] and k [W/m · K] are the constant values for heat capacity at constant pressure, and thermal conductivity, respectively. These local properties depend of materials for each subdomain in the system. Moreover, T [K] is the local temperature, $\mathbf{u}$ [m/s] is the velocity field, and $\mathbf{q}_e$ [W/m^3] is the heat power flux generated by an electronic device inside the system. For the entire model $\mathbf{q}_e = P_e/V_t$ and for the reduced model $\mathbf{q}_e = P_e/V_S$. Since P_e [W] is the total heat power produced by the unknown device of volume V_t [m^3]. This volume is sliced in N_S such volumes V_S ($V_S = V_S / V_t$ [m^3]) for the reduced computational domain.

The first *l.h.s.* term of eq. (9) represents the system temperature changes; whilst the *r.h.s.* terms refer to the heat transfer rate due to the conduction mechanism (Fourier's law), and the energy generation rate inside the system. Also, it is important to remark that $\partial T/\partial t = 0$ [K/s], in eq. (9), when the process is analysed in steady state, as well as $(\mathbf{u}\cdot\nabla)T = 0$ [K/s] for the solid subdomains.

Besides mass and energy balances, eqs. (8) and (9), the behaviour of fluids through their velocity fields has to be described. This associated physical problem is coupled with the heat transfer problem for an accurate description of the natural or free convection process. Hence, in this work any external source of fluid motion is disregarded, and only the gravitation effect is considered. The fluid mechanic problem is stated by using Navier-Stokes equations [15, 19], with the Boussinesq approximation and assuming Newtonian and laminar fluids, as shown,

$$\rho\left[\frac{\partial \mathbf{u}}{\partial t} + (\mathbf{u}\cdot\nabla)\mathbf{u}\right] = -\nabla p + \mu\nabla^2\mathbf{u} + \beta\mathbf{g}(T - T_0), \tag{10}$$

since ρ [kg/m^3] is the mass density at the reference temperature T_0 [K], p [Pa] is the pressure field, β [1/K] is the coefficient of thermal expansion, μ [Pa · s] is the dynamic viscosity, $\mathbf{g}$ [m/s^2] is the local gravitational acceleration vector. The inertial forces in the *l.h.s.* of eq. (10) are balanced by the pressure, viscous, and external forces in the *r.h.s.* This latter term is also known as the buoyancy force due to the gravity.

Summarising, the mathematical model is defined by eqs. (8) to (10), and their three unknown variables, T, p and $\mathbf{u}$. The required boundary conditions to solve these stationary and transient problems are presented as follows. Fig. 2 displays boundary conditions for the reduced model such as: symmetry, isothermal, adiabatic, heat source, and slip conditions. The first set of boundary conditions which deals with the reduced model symmetry at its internal boundaries (Fig. 2), is

$$\mathbf{n}\cdot\mathbf{q} = 0, \tag{11}$$

$$\mathbf{n}\cdot\mathbf{u} = 0, \tag{12}$$

where $\mathbf{n}$ is the normal unit vector of an internal face. Similarly, the adiabatic conditions, akin eq. (11), are defined at the axial symmetric edge, and at the bottom boundary of the computational domain. Conditions at walls for fluid subdomains in Fig. 2 are set as slip boundaries like eq. (12). External faces of the system are established with the isothermal condition (Fig. 2) as

$$T = T_a, \tag{13}$$

since T_a [K] is the ambient temperature. Moreover, the subdomain (e), from Fig. 1, is assumed as the heat power source or unknown electronic device. Lastly, initial conditions for transient studies are defines such as

$$T(t=0) = T_a, \tag{14}$$

$$\mathbf{u}(t=0) = \mathbf{0}, \tag{15}$$

and

$$p(t=0) = p_0. \tag{16}$$

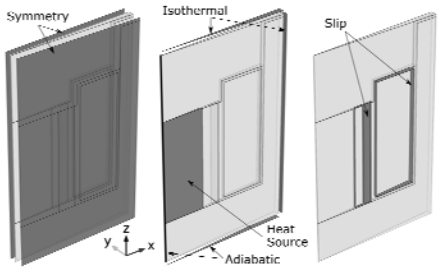

Fig. 2 – Boundary conditions of the reduced computational domain: (left) symmetry, (centre) isothermal, adiabatic, heat source, and (right) slip conditions.

4. METHODOLOGY

The mathematical problem stated above, for both stationary and transient states, was solved numerically via the finite element method. Fig. 3 exhibits the computational domain mesh implemented in this work. This mesh was conformed for 26 155 tetrahedral elements, 13 017 triangular elements, 1 027 edge elements, and 40 vertex elements. Numerical tasks were executed in a CPU with Dual Core AMD® Opteron™ Processor 275, 3 out of 4 cores, and using Linux as operating system. In all performed simulations $T_0 = T_a = 298.15$ K, $N_S = 140$, $\mathbf{g} = (0,0,-9.81)^T$ m/s^2, and $p_0 = 101325$ Pa.

Simulations carried out were grouped in six systematic sets, whose details are described in *Table 2*. The insulation column is related to the kind of insulation employed, *i.e.*, practical or ideal. For a practical insulation, it is assumed Polystyrene for subdomains (a) and (b), from Fig. 1, otherwise, the system is supposed isolated (or ideally insulated). Also, last column means whether the fluid motion effect in the heat transfer process was included. In other words, it says if the problem is completely a conductive one.

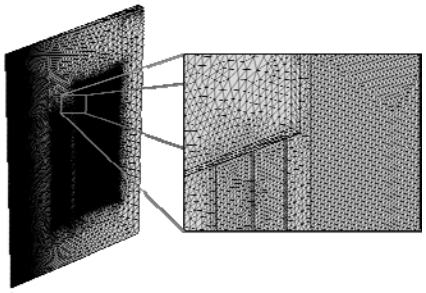

Fig. 3 – Computational domain mesh of the studied system.

Table 2

The features of each set of simulations that are carried out

Set	Time State	P_e [W]	Insulation	Fluid Motion
1	Stationary	0.1	Practical	Included
2		[0.001,0.1]		
3	Transient	[0.001,0.1]	Practical	Included
4				Disregarded
5			Ideal	Included
6				Disregarded

5. RESULTS AND DISCUSSION

Figure 4 presents the velocity field of the air in the main chamber, and the water in the reservoir, under stationary conditions with 0.1 W of total heat power (set 1 from Table 2). It is noticed the well-known convection cell due to the thermal power flux passing through the system. Moreover, this motion has a low scale at the reservoir filled with the working fluid. As it is observed, its maximum value is 2.01×10^{-3} m/s compared against 0.28 m/s from the air velocity maximum value. This value brought it up hints about the multiphysical problem could be approximated to a purely conductive heat transfer problem.

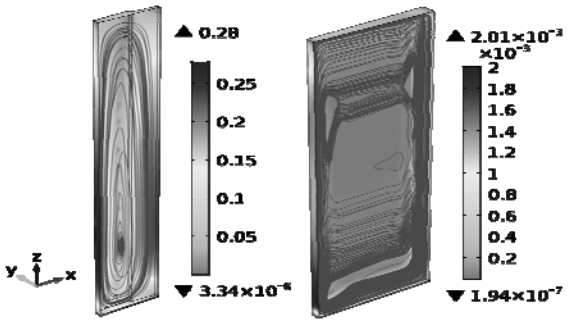

Fig. 4 – Velocity fields **u** [m/s] of fluids from results of simulation set 1: (left) air, and (right) water.

Figure 5 shows the heat power distribution per unit area, the heat flux magnitude (q'' [W/m^2]), inside the domain under stationary conditions. It is observed that fluxes reach the working fluid as is expected in a calorimetry-based apparatus. Altogether, velocity and heat flux magnitude distributions have a narrow relationship with a measurable quantity, *i.e.*, the temperature. Temperature difference distribution θ [°C] of the reduced computational domain is also exhibited in Fig. 5. Further, it is noticeable an almost homogeneous distribution of θ about 27 °C for water body, unlike temperature values in the main chamber. It is said because the water temperature distribution range is 0.3 °C, with maxima located in bottom vertices. These positions can be temperature sensor placements for an eventual real implementation.

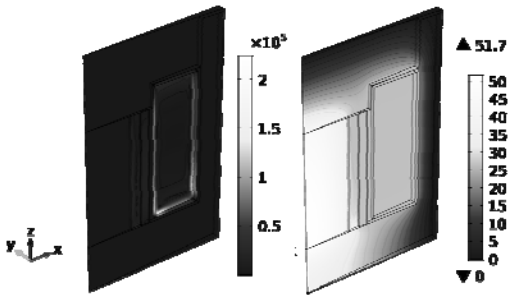

Fig. 5 – Distributions of the (left) heat flux magnitude q'' [W/m^2], and (right) temperature difference θ [°C], from results of simulation set 1.

Subsequently, the second set of simulations, described in Table 2, was carried out, and its results are detailed in Table 3. That is the average temperature difference for both fluids, air and water, which fill the main chamber and the reservoir, respectively, varying the heat power. Also, the measured temperatures at the bottom vertex of each chamber are appended. It is easy to calculate the slope of each temperature difference measurement, in function of heat power and utilising data from Table 3. This slope corresponds to the thermal resistance model, R [K/W], in eq. (4). R values are displayed in Table 4 as a first numerical approximation to the real system operation. In stationary state when the storage body is fully charged R is principally linked with the heat flux path and the insulation.

Table 3

Temperature difference (θ) values of several measurements, for different values of the total heat power. These are the average values for air, and water; and point values in the bottom vertices at the main chamber, and the reservoir

P_e [W]	$\theta_{avg,air}$ [°C]	$\theta_{avg,water}$ [°C]	θ_{MC} [°C]	θ_R [°C]
0.001	0.3756	0.2643	0.2675	0.2647
0.005	1.6128	1.3107	1.3273	1.3142
0.010	3.0814	2.6312	2.6638	2.6391
0.050	14.3030	13.1095	13.2570	13.1556
0.100	28.3445	26.5027	26.7839	26.5983

Table 4

Equivalent thermal resistance values determined between different locations of the system under stationary conditions

Location	θ [°C]	R [K/W]
Air in the main chamber	$\theta_{avg,air}$	281.7559
Main chamber bottom vertex	$\theta_{avg,water}$	267.6173
Water in the reservoir	θ_{MC}	264.8150
Reservoir bottom vertex	θ_R	265.7795

Once stationary analyses were performed, transient simulations specified in *Table 2*, such as sets 3 to 6, were carried out. In these studies the heat power, P_e, was varied assuming four sceneries from combining whether the fluid motion is included and, whether the insulation material is either practical (Polystyrene) or ideal (isolation). Results in terms of the temperature difference, θ [°C], at the reservoir bottom vertex as a function of time are displayed in Figs. 6 to 9 from sets 3 to 6, respectively. A slightly difference between results from sets 3 and 4 (Figs. 6, 7) and between the couple of sets 5 and 6 (Figs. 5, 6) is noticeable. This difference from both couples is mainly due to the fact of disregard the fluid motion (Navier-Stokes equations), during the heat transfer problem simulation. The principal reason for only dealt with thermal conduction was discussed around Fig. 4. By comparing the second couple against the first one, it is clear the influence of assuming an ideal insulation material, or $R \propto \theta_\infty \to \infty$. This last relationship indicates the system is slowly going to blow up at any time. Hence, the power estimation should be performed in a finite time much before water reaches its boiling point, and the electronic circuit is jeopardised, *i.e.*, $t << 15 \times 10^{15}$ s. For practical implementation, this is more than enough to acquire plenty data for an accurate estimation.

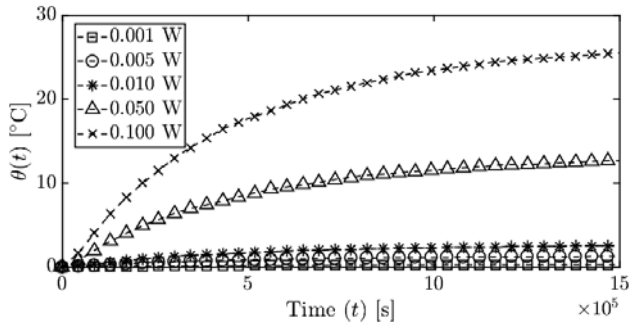

Fig. 6 – Temperature difference θ [°C] measured in a point inside the reservoir filled with water, from results of simulation set 4.

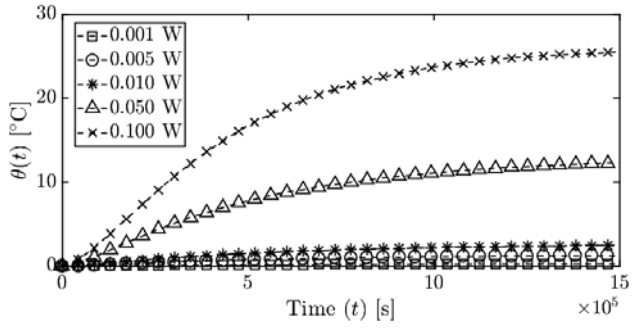

Fig. 7 – Temperature difference θ [°C] measured in a point inside the reservoir filled with water, from results of simulation set 5.

Table 5 presents average and standard deviation of errors calculated for both couples of temperature measurements though. It is notorious the error value increases when the heat power rises either, because fluid motion becomes important, and boosts the convective heat transfer process. Thus, the heat conductive approach, employed in sets 4 and 6, is appropriate for microelectronic devices with low power losses. However, this error is related to a magnitude factor, which can be rectified through calibration and tuning procedures of a practical implementation.

Furthermore, Fig. 9 is obtained by extending results from the last set of simulations, whose considers ideal insulation and disregards fluid motion phenomenon. It shows how the temperature slope is augmented through the heat power increasing, which reduces the available time for estimation. These results are considered the desired behaviour for a calorimetric application. Therefore, it is possible to obtain the estimated heat power, $\dot{Q}$, from eq. (7) and employing thermophysical properties for water in Table 1, as is shown in Fig. 10. Estimated power losses are close to assumed heat powers as sources, with a logarithmic rise of magnitude error. Nonetheless, this error can be measured and adjusted in a real implementation, as it was mentioned before. Certainly, a quite good insulation must be guaranteed, as much as an ideal one. Furthermore, there were detected additional mechanisms to enhance the performance of the proposed non-conventional calorimeter, which are going to be explored in future works, such as: incorporate colloids with electromagnetic susceptibility as working fluids, include a fin array inside the reservoir of fluid, and apply non-mechanical external forces, for example.

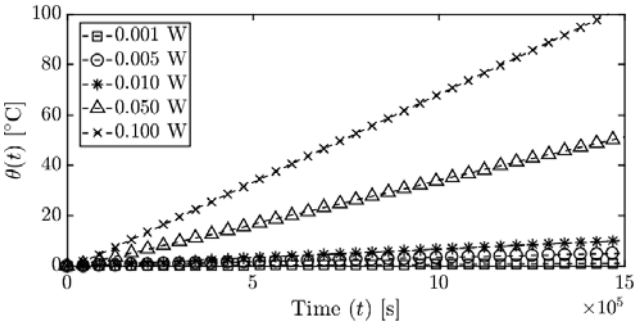

Fig. 8 – Temperature difference θ [°C] measured in a point inside the reservoir filled with water, from results of simulation set 6.

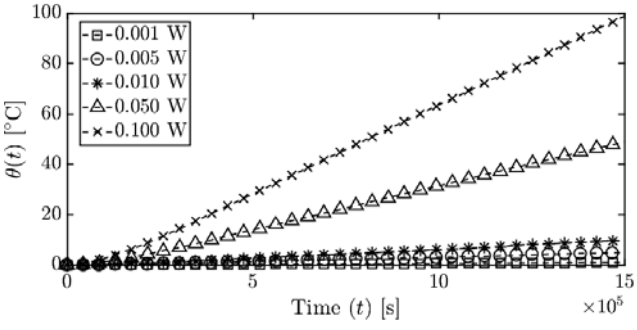

Fig. 9 – Temperature difference θ [°C] measured in a point inside the reservoir filled with water, from results of simulation set 6.

Table 5

Average and standard deviation of errors, calculated for the two couples (sets 3–4 and 5–6) of temperature differences, varying the heat power (P_e)

P_e [W]	$\varepsilon = \theta_3 - \theta_4$ [°C]	$\varepsilon = \theta_5 - \theta_6$ [°C]
	$\varepsilon_{avg} \pm \varepsilon_{std}$ [°C]	
0.001	0.0145 ± 0.0072	0.0300 ± 0.0075
0.005	0.0525 ± 0.0366	0.2123 ± 0.0488
0.010	0.1230 ± 0.0753	0.4493 ± 0.0992
0.050	0.5772 ± 0.3224	2.2927 ± 0.4776
0.100	0.4865 ± 0.8675	4.2590 ± 0.8975

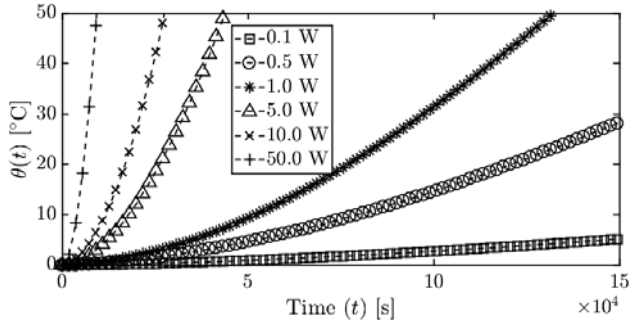

Fig. 9 – Temperature difference θ [°C] measured in a point inside the reservoir filled with water, from results of simulation set 6.

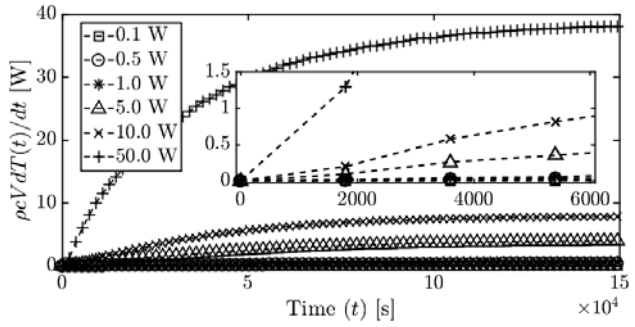

Fig. 10 – Estimated power losses $\hat{Q}$ [W] using measurements in a point inside the reservoir filled with water and its thermophysical properties, from results employing conditions of set 6.

6. CONCLUSIONS

A non-conventional calorimeter for electronic devices was proposed, and its early numerical simulations and analyses were performed. The studied system was mainly conformed by a vertical cylindrical concentric cavity, based on the constant-volume calorimetry principle. The numerical simulations were organised in six sets. The first two conveyed information about the stationary response of the calorimetric system varying the power losses. The first set evidenced that heat transfer inside the inner air space occurs mainly through conduction (the convection flow maximum value ~2.01×10^{-3} m/s is much less than the air velocity maximum value 0.28 m/s). An almost uniform temperature for the water body (~27 °C) was noticed, unlike inside the main chamber. The water temperature range is 0.3 °C, with maxima located by the vertices at the bottom. These positions are candidate for temperature sensor placements in an eventual real implementation. In addition, the equivalent thermal resistance shows off higher values in stationary state (Table 4). A high insulation level is then needed to prevent heat flux leakage. Likewise, a slow motion of the working fluid (water) was observed, which prevents a possible reduction of the system complexity. This modification is a consequence of treating the problem as purely heat conduction, and of assuming ideal insulation instead of a real insulating material. It represented the foundation of further analyses, that is sets 3 to 6, which address whether the fluid motion effect is considered, and whether either practical (Polystyrene) or ideal insulation is employed. It was identified that the problem can be approached as one of conductive type, assuming an ideal insulation, and using low power losses from microelectronic devices. Hence, the power estimation should be performed in a finite time, long before water reaches its boiling point and the electronic circuit is menaced. Subsequently, power losses were estimated for several illustrative examples, which showed to be good approaches. The errors perceived (Table 5) are attributed to the level of approximation, strongly related to the heat power magnitude. Nevertheless, it is worthy to mention these error values can be adjusted through the calibration and tuning process. Therefore, it may be inferred that the desired operation of the system, in the heat transfer sense and using an insulation coat as ideal as possible, relays on trying to "*slowly burn the system up*". This research opened the door to further works aimed to enhance the performance and estimation quality of the proposed non-conventional calorimeter.

ACKNOWLEDGEMENTS

This work has been supported by the *Consejo Nacional de Ciencia y Tecnología* (CONACyT) of Mexico, under the grant number 578594. Furthermore, we thank to the direction and the electronic engineering department of the *Disivión de Ingenierías del Campus Irapuato-Salamanca* from the University of Guanajuato, and to the Laboratory for Multiphysics Modeling at the faculty of Electrical Engineering of The "Politehnica" University of Bucharest.

Received July 17, 2017

REFERENCES

1. X. Chen, H. Ye, X. Fan, T. Ren, G. Zhang, *A review of small heat pipes for electronics*, Appl. Therm. Eng., **96**, pp. 1–17 (2016).
2. C. Green *et al.*, *A Review of Two-Phase Forced Cooling in Three-Dimensional Stacked Electronics: Technology Integration*, J. Electron. Packag., **137**, *4*, p. 9 (2015).
3. P.D. Malliband, *Design of a double-jacketed, closed type calorimeter for direct measurement of motor losses*, Seventh International Conference on Power Electronics and Variable Speed Drives, London, UK, 21–23 Sept. 1998.
4. C.X.C. Xiao, G.C.G. Chen, W.G.H. Odendaal, *Overview of Power Loss Measurement Techniques in Power Electronics Systems*, IEEE Trans. Ind. Appl., **43**, *3*, pp. 657–664 (2007).
5. L. Yang, S. Liming, L. Yaohua, *Comparison analysis of loss calculation methods and measurement techniques in power electronics and motor systems*, International Conference on Electrical Machines and Systems (ICEMS), Busan, South Korea, 26–29 Oct. 2013.
6. W. Hemminger, S.M. Sarge: *Thermal Analysis and Calorimetry*, in: K. Gallagher, M.E. Brown, R.B. Kemp (Edit.), *Handbook of Thermal Analysis and Calorimetry*, Amsterdam, The Netherlands, Elsevier, 1999, pp. 7–30.
7. J. P. McCullough, D. W. Scott, *Calorimetry of Non-Reacting Systems: Prepared Under the Sponsorship of the International Union of Pure and Applied Chemistry Commission on Thermodynamics and the Thermochemistry*, Elsevier, London, UK, 2013, pp. 1–13.
8. F. Blaabjerg, J.K.K. Pedersen, E. Ritchie, *Calorimetric measuring systems for characterizing high frequency power losses in power electronic components and systems*, IEEE Industry Applications Conference, 37th IAS Annual Meeting (Cat. No.02CH37344), Pittsburgh, USA, 13–18 Oct. 2002.
9. P.D. Malliband, N.P. Van Der Duijn Schouten, R.A. McMahon, *Precision calorimetry for the accurate measurement of inverter losses*, Proc. Int. Conf. Power Electron. Drive Syst., **1**, pp. 321–326 (2003).

10. S. Weier, M.A. Shafi, R. McMahon, *Precision calorimetry for the accurate measurement of losses in power electronic devices*, IEEE Trans. Ind. Appl., **46**, *1*, pp. 278–284 (2010).
11. D. Christen, U. Badstuebner, J. Biela, J.W. Kolar, *Calorimetric power loss measurement for highly efficient converters*, Int. Power Electron. Conf. (IPEC), Sapporo, Japan, 21–24 Jun. 2010.
12. J. Marín, D. Tibaduiza, R. Correa, *Determinación experimental de la cantidad de calor emitido por un circuito electrónico*, Rev. Ing. Univ. Medellín, **11**, *20*, pp. 191–202 (2012).
13. D.F. Frost, D.A. Howey, *High-speed Peltier calorimeter for the calibration of high-bandwidth power measurement equipment*, IEEE Trans. Instrum. Meas., **65**, *1*, pp. 155–163 (2016).
14. Y.A. Cengel, M.A. Boles, *Thermodynamics: an engineering approach*, 5th ed., McGraw-Hill, New York, 2006, pp. 165–218.
15. A. M. Morega, *Principles of Heat Transfer*, in: D.B. Marghitu (Edit.), *Mechanical Engineer's Handbook*, Academic Press, San Diego, USA, 2001, pp. 445–557.
16. T.L. Bergman, F.P. Incropera, D.P. DeWitt, A.S. Lavine, *Fundamentals of heat and mass transfer*, 7th ed., John Wiley & Sons, Inc., Jefferson City, 2011, pp. 279–346.
17. F. Kreith, R. M. Manglik, M. S. Bohn, *Principles of Heat Transfer*, 7th ed., Cengage Learning, Stamford, USA, 2011, pp. 70–333.
18. A. Bejan, *Advanced engineering thermodynamics*, 3rd ed., John Wiley & Sons, Inc., New York, USA, 2006, pp. 1–39.
19. R.B. Bird, W.E. Stewart, E.N. Lightfoot, *Transport Phenomena*, 2nd ed., John Wiley & Sons, Inc., New York, USA, 2006, pp. 333–361.